

Unraveling siRNA Unzipping Kinetics with Graphene

Santosh Mogurampelly¹, Swati Panigrahi², Dhananjay
Bhattacharyya², A. K. Sood³, and Prabal K. Maiti^{1*}

¹*Centre for Condensed Matter Theory, Department of Physics,
Indian Institute of Science, Bangalore 560012, India*

²*Biophysics Division, Saha Institute of Nuclear Physics, Kolkata 700064, India*

³*Department of Physics, Indian Institute of Science, Bangalore 560 012, India*

Abstract

Using all atom molecular dynamics simulations, we report spontaneous unzipping and strong binding of small interfering RNA (siRNA) on graphene. Our dispersion corrected density functional theory based calculations suggest that nucleosides of RNA have stronger attractive interactions with graphene as compared to DNA residues. These stronger interactions force the double stranded siRNA to spontaneously unzip and bind to the graphene surface. Unzipping always nucleates at one end of the siRNA and propagates to the other end after few base-pairs get unzipped. While both the ends get unzipped, the middle part remains in double stranded form because of torsional constraint. Unzipping probability distributions fitted to single exponential function give unzipping time (τ) of the order of few nanoseconds which decrease exponentially with temperature. From the temperature variation of unzipping time we estimate the energy barrier to unzipping.

*To whom correspondence should be addressed; Electronic address: maiti@physics.iisc.ernet.in

I. INTRODUCTION

The interaction of nucleic acids with carbon nanotubes (CNTs) and graphene have attracted much attention due to the potential applications in nanotube separation [1, 2], sensing [3, 4], sequencing [5–7] and nanomedicine [8–11]. Basic understanding of the interaction mechanism of nucleic acids with CNT or graphene [12–17] is essential for such applications. Small interfering ribonucleic acid (siRNA) molecules are a class of double stranded non-coding RNA which are typically 21 to 23 nucleotides in length. The properties of siRNA are actively being studied due to their potential influence on cell functionality and applications in medicine to achieve RNA interference (RNAi) [18–20]. The mechanism of RNAi involves RNA-induced silencing complex (RISC) comprising of Dicer, Argonaute2 and siRNA binding protein that induces unzipping of siRNA into two single strand RNAs [21–25]. One of these two strands acts as a guiding strand to form specific base-pairs with mRNA and silences the gene. For using RNAi technology in the treatment of diseases such as cancer, HIV, viral infections and eye diseases [26], efforts are being made for the efficient and safe siRNA delivery systems to achieve the desired RNAi effect. Dendrimers [27–29] and carbon nanotubes [8–10, 15] are good carriers of siRNA into disease infected cell. The discovery of graphene has led to its possible use in efficient delivery of siRNA as well as various oligonucleotides. Several attempts have been made to study the properties of nucleic acid interaction with graphene [4, 11, 13, 14, 17, 30, 31]. However the interaction between graphene and siRNA/DNA has not been understood.

In this paper, we show the unzipping of siRNA on graphene and subsequent binding between the two. Graphene is a free-standing two dimensional monolayer of carbon atoms arranged into a honeycomb lattice [32, 33]. Graphene is a partially hydrophobic molecule: its faces are highly hydrophobic while edges, depending on functionalization, can be hydrophilic in nature [34]. Thus it has the ability to pass through hydrophobic lipid bilayer and can also interact with the hydrophilic head groups. Dispersion interaction including $\pi - \pi$ stacking serves as the major attractive interactions between the non-polar molecules [35]. The importance of dispersion interactions has been verified recently in analyzing the structure and energetics of the graphene-nucleobase complexes [36] and in studying the unzipping of siRNA with single walled CNT [15]. Using state of the art all atom molecular dynamics simulation along with the *ab-initio* quantum mechanical calculations, we give a comprehensive understanding of the structure and

thermodynamics of the siRNA-graphene complex. In the supplementary material [37], we discuss the effect of force fields (FF) on the unzipping and adsorption of siRNA/dsDNA on graphene.

II. COMPUTATIONAL DETAILS

A. Classical simulations

We have used AMBER11 suite of programs [38] for simulating the systems with Amber 2003 (along with ff99) force fields [39] and the TIP3P model [40] for water. Latest improvements of torsion angle parameters are reported for DNA/RNA in a new force field called parmbsc0 and ff10 [41–43]. The comparison of force fields ff99, parmbsc0 and ff10 are discussed in the supplementary material. Similar conformational changes are observed with ff99, parmbsc0 and ff10. Use of ff99 also helps us to compare the present results with our previous simulations on siRNA-dendrimer complex that used ff99 [29]. The initial structure of the small interfering ribonucleic acid (siRNA) was taken from the protein data bank (PDB code: 2F8S)[44]. The sequence of the siRNA used is r(UU AGA CAG CAU AUA UGC UGU CU)₂ with sticky ends of sequence UU on the two ends of the strands. We have built graphene sheet of $140 \times 140 \text{ \AA}^2$ wider dimensions to ensure sufficient sliding area for the siRNA before optimum binding on graphene. For comparison, we have also simulated dsDNA of the same length on graphene. The dsDNA has same sequence as the siRNA where the nucleobase Uracil (U) is replaced by Thymine (T) nucleobase, *i.e.*, d(TT AGA CAG CAT ATA TGC TGT CT)₂. Structure of the dsDNA in B-form was generated using NUCGEN module of AMBER [38]. The siRNA/dsDNA-graphene complex structure is then solvated with TIP3P model water box using the LEaP module in AMBER 11 [38]. The box dimensions were chosen such that there is at least 20 Å solvation shell from the surface of siRNA/dsDNA-graphene complex to the edge of the water box. In addition, some water residues were replaced by 44 Na⁺ counterions for siRNA and 42 Na⁺ counterions for dsDNA to neutralize the negative charge on the phosphate backbone groups of the siRNA/dsDNA structure. This has resulted in box dimensions of $188 \times 186 \times 72 \text{ \AA}^3$ with total system size of 214602 atoms for siRNA-graphene complex and $188 \times 186 \times 69 \text{ \AA}^3$ with total system size of 206865 atoms for dsDNA-graphene complex. The crystal structure of siRNA and the initial system containing siRNA and graphene with added water plus neutralizing counterions are shown in Figures 1(a)

and 1(b), respectively.

We have modeled the carbon atoms in graphene as uncharged Lennard-Jones particles with LJ parameters listed in Table I. The bonded interactions viz., stretching, torsion and dihedral terms were also included. To keep the graphene fixed during simulations, all the carbon atom positions in graphene were restrained with harmonic potential of spring constant of 1000 kcal/mol-Å². The translational center of mass motions were removed every 1000 steps. The system is subjected to standard simulation protocol described in Refs. [45, 46]. The long range electrostatic interactions were calculated with the Particle Mesh Ewald (PME) method [47] using a cubic B-spline interpolation of order 4 and a 10⁻⁵ tolerance is set for the direct space sum cutoff. A real space cutoff of 9 Å was used both for the long range electrostatic and short range van der Waals interactions with a non-bond list update frequency of 10. The trajectory was saved at a frequency of 2 ps for the entire simulation scale of 55-85 ns for each system. We have used periodic boundary conditions in all three directions during the simulation. Bond lengths involving bonds to hydrogen atoms were constrained using SHAKE algorithm [48]. This constraint enabled us to use a time step of 2 fs for obtaining long trajectories of each 50 ns. During the minimization, the siRNA/dsDNA-graphene complex structures were fixed in their starting conformations using harmonic constraints with a force constant of 500 kcal/mol-Å². This allowed the water molecules to reorganize which eliminates bad contacts with the siRNA/dsDNA and the graphene. The minimized structures were then subjected to 40 ps of MD, using 1 fs time step for integration. During the MD, the system was gradually heated from 0 to 300 K using weak 20 kcal/mol-Å² harmonic constraints on the solute to its starting structure. This allows slow relaxation of the siRNA/dsDNA-graphene complex structure. Subsequently, simulations were performed under constant pressure-constant temperature conditions (NPT), with temperature regulation achieved using the Berendsen weak coupling method [49] (0.5 ps time constant for heat bath coupling and 0.5 ps pressure relaxation time). Constant temperature-pressure MD was used to get the correct solvent density corresponding to experimental condition. Finally, for analysis of structures and properties, we have carried out 50 ns of NVT production MD with 2 fs integration time step using a heat bath coupling time constant of 1 ps.

The binding free energy for the non-covalent association of two molecules in solution can be written as $\Delta G(A + B \rightarrow AB) = G_{AB} - G_A - G_B$. For any species on the right hand side $G(X) =$

$H(X) - TS(X)$, accordingly,

$$\Delta G_{bind} = \Delta H_{bind} - T\Delta S_{bind} \quad (1)$$

where $\Delta H_{bind} = \Delta E_{gas} + \Delta G_{sol}$. Here ΔH_{bind} is the change in enthalpy and is calculated by summing the gas-phase energies (ΔE_{gas}) and solvation free energies (ΔG_{sol}); $E_{gas} = E_{ele} + E_{vdw} + E_{int}$, where E_{ele} is the electrostatic energy calculated from the Coulomb potential, E_{vdw} is the non-bond van der Waals energy and E_{int} is the internal energy contribution from bonds, angles and torsions. $G_{sol} = G_{es} + G_{nes}$ where G_{es} is the electrostatic energy calculated from a Generalized Born (GB) method and G_{nes} is the non-electrostatic energy calculated as $\gamma \times SASA + \beta$; where γ is the surface tension parameter ($\gamma = 0.0072 \text{ kcal/mol-}\text{\AA}^2$), $SASA$ is the solvent-accessible surface area of the molecule and β is the solvation free energy for a point solute ($\beta = 0$). For the entropy calculation we have used two-phase thermodynamic (2PT) model [50, 52, 53], based on density of states (DoS) function. The DoS function can be calculated from the Fourier transform of the velocity auto-correlation function which provides information on the normal mode distribution of the system. The method has found successful application in several related problems [50–54].

B. Quantum simulations

We have carried out quantum chemical calculations to understand the interaction of the planar nanographene with the nucleosides of RNA and DNA. For the present investigation, we have taken a graphene sheet of (6×6) dimension with alternate armchair and zig-zag edges with C-C bond lengths of 1.42 \AA , C-H bond length 1.09 \AA and all the angles kept at 120° . The edges are terminated with hydrogen atoms to avoid any unwanted terminal effects [55]. We have modeled adenine, guanine, cytosine, thymine and uracil with furanose sugar connected to the respective nucleobases by the β -glycosidic bond. As structural features that distinguish siRNA from DNA are the presence of uracil nucleobase and hydroxyl-OH group in the constituted ribose sugar in siRNA, we have modeled thymine with the deoxyribose sugar and all other bases are modeled with ribose sugar to be consistent with siRNA structure. These structures act as miniature models of siRNA and DNA to understand the interaction with the planar graphene molecule. Initially the nucleosides are placed vertically above, around 4 \AA from the center of the planar hexagonal ring of the graphene and the nucleobases lie parallel to the graphene sheet. All the model building was done with the help of Discovery studio 2.0 [56] and Molden [57] software.

We have optimized all the graphene-nucleosides complex systems to get the energy minimized configuration. For all the quantum chemical calculations, we have employed dispersion corrected density functional approach using ω B97XD/6-31G** basis set[58] using Gaussian 09 [59] . The total interaction energy of each system has been calculated using $E_{int} = E(\text{complex}) - EX_o(\text{isolated graphene}) - EY_o(\text{isolated nucleoside}) + \text{BSSE}$, where BSSE represents basis set superposition error, arising from the overlapping of the atomic orbitals. The BSSE corrections has been calculated using Boys and Bernardi function counterpoise method [60] . We have also carried out frequency calculation on the optimized geometry using the same method and basis set. To analyze the degree of binding, we have also carried out the charge transfer analysis of the nucleosides and graphene sheet using the Natural Bond Orbital (NBO) approach [61–63] .

III. RESULTS AND DISCUSSION

A. siRNA Unzipping

Figure 1(c) shows the instantaneous snapshots of siRNA as it binds to graphene. The unzipping of base-pairs starts within 3 ns and by 22 ns, 41 of the initial 48 Watson-Crick (WC) H-bonds are broken resulting in almost complete unzipping of siRNA into two single strand RNAs. Figure 2 shows the number of intact H-bonds of siRNA and dsDNA with time when bound to graphene. Breaking of WC H-bonds in siRNA/dsDNA manifest the deformation mechanism of nucleic acid molecule [64–66]. It can be seen that a large decrease of H-bonds occurs in the first few nanoseconds when siRNA starts unzipping and within 22 ns, 41 H-bonds are broken leaving only 7 intact H-bonds. The unzipped bases are then free to interact with graphene surface via van der Waals forces. Figure 2 shows that H-bonds are saturated at 7. At this stage, siRNA optimally binds to graphene and the complex is very stable after 22 ns. In the optimum bound configuration where H-bonds are constant with time, there are few transient H-bonds due to room temperature thermal fluctuations. Because of these transient H-bonds, the curve has fluctuations about its mean value with standard deviations ranging from 1 to 3 H-bonds. The different nucleosides interact with different strength with graphene making the binding possible. Interestingly, dsDNA of same sequence and length show much less unzipping and binding on graphene compared to siRNA.

Within 6 ns, only 8 of total 48 H-bonds in dsDNA get unzipped and remain constant at 40 H-bonds throughout the rest of simulation time of 44 ns. This difference has its origin in the extra hydroxyl group of uridine that is present in siRNA. To have a molecular level understanding of this binding affinity we calculate the binding free energy of different nucleosides with graphene both from the classical MD simulations (using MM-GBSA method) as well as from our dispersion corrected DFT calculations.

B. Binding free energy

Figure 3 shows the enthalpy contribution to the total binding free energy as a function of time as siRNA binds to graphene. In the plot, we have marked the time interval at which optimal binding happens as reflected by the binding energy. After this binding the complex is stable for the entire duration of the simulation with fluctuations ranging only 1.5 % of its average value in the optimum bound state. From the stable trajectory of siRNA-graphene complex, the enthalpy contribution (ΔH_{bind}) to the total binding free energy was calculated for 250 snapshots separated each by 2 ps. The enthalpy contribution (ΔH_{bind}) to the total binding free energy is -562.6 ± 6.2 kcal/mol. Entropy is calculated at every 5 ns along the trajectory. For this, we simulate the system for 40 ps with velocities and coordinates saved at a frequency of 4 fs. The velocity auto-correlation function converges within 10 ps. When siRNA is binding with graphene during initial stage, siRNA entropy decreases since the graphene substrate suppress the fluctuations of unzipped bases (inset of Figure 3). After siRNA binds optimally to graphene, the entropy starts increasing again due to inherent kinetics of unzipped bases. However the entropy contribution ($T\Delta S_{bind}$) to the total binding free energy is small compared to the enthalpy contribution (ΔH_{bind}) arising due to dispersive interaction between the graphene and the aromatic nucleobases. The enthalpy and entropy contributions in Eqn. 1 give the total binding free energy (ΔG_{bind}) of siRNA when binding to graphene. The value of ΔG_{bind} is -573.0 ± 8 kcal/mol. However, the binding energy of the dsDNA bound to graphene is calculated to be -190 ± 9 kcal/mol which is very low compared to siRNA bound to graphene.

To get further molecular level picture of the binding mechanism we also compute the histograms of the closest approach of nucleoside to graphene. This will allow us to understand the relative binding affinity as well as how different nucleosides are oriented on the graphene

substrate. We track the center of mass position of different nucleobases with respect to graphene as a function of simulation time. We calculate the closest approach of nucleoside to graphene as the perpendicular distance $r_{\perp} = \hat{z} \cdot \overrightarrow{AB} = B_z - A_z$ (because graphene is in $x - y$ plane) where A and B are the centers of mass position of nucleoside and graphene, respectively. r_{\perp} is calculated for 50 ns trajectory and the histogram of nucleosides is shown in Figure 4(a). From this plot, we can understand the probability ($P(r_{\perp})$) of finding the nucleoside at a given position r_{\perp} from the graphene. Using histogram, the free energy of nucleoside is calculated as $F(r_{\perp}) = -k_B T \ln(P(r_{\perp}))$ (where k_B is the Boltzmann constant) and plotted as a function of distance in Figure 4(b). The minimum in the free energy indicates the most optimum bound configuration for nucleoside-graphene complex. In the inset we show the zoomed part of the occurrence of free energy minima. $F(r_{\perp})$ has minima at 3.775 Å , 3.790 Å , 3.795 Å , 3.840 Å and 3.860 Å for guanosine, Thymidine, adenosine, uridine and cytidine, respectively. Guanine can form strongest H-bonding interaction and stacking interaction with graphene. The distance of closest approach in the increasing order for guanosine, thymidine, adenosine, uridine and cytidine is $r_{\text{opt}}(G) < r_{\text{opt}}(T) \sim r_{\text{opt}}(A) < r_{\text{opt}}(U) < r_{\text{opt}}(C)$. Hence guanine has most interaction strength with graphene and cytidine has least interaction strength as $G > T \sim A > U > C$. The binding energy order of nucleosides is consistent with experimental and theoretical calculations [12–14]. The stable complex structure with most of the base-pairs already unzipped in siRNA can be delivered to the target virus infected cell for RNAi applications. Since siRNA has to undergo unwinding process with the effect of RISC, our proposed delivery mechanism by graphene possesses potential advantages in achieving RNAi. Toxic effects of graphene inside cell may be suppressed with proper surface functionalization [67–69].

C. Structural deformation

Snapshots shown in Figure 1 indicate that the siRNA molecule exhibit large structural deformation on binding to graphene. This structural deformation is characterized by the number of siRNA atoms that come close to the graphene in a specified cutoff distance and the root mean square deviation (RMSD) of siRNA with respect to its crystal structure. We calculate close contacts N_c when any siRNA atoms are within 5 Å of the graphene sheet. The number of close contacts N_c between siRNA and graphene is plotted in Figure 5(a) as a function of

time. Since siRNA is getting unzipped within 21 ns, N_c is increasing rapidly within 21 ns and reaches a constant value of 710 siRNA atoms. The fluctuations are very less in N_c after the complete binding of siRNA to the graphene. Interestingly, for dsDNA N_c is much less than that of siRNA. The dsDNA has only 240 atoms within 5 Å from graphene sheet in the stable configuration. This also demonstrates very low binding affinity of dsDNA compared to siRNA with graphene. In Figure 5(b) we plot the RMSD of siRNA/dsDNA as a function of time for both the siRNA/dsDNA-graphene complex. For the calculation of RMSD, the reference structure of siRNA is taken to be the crystal structure of siRNA after initial minimization. Note that the plot shows RMSD for only production NVT simulation time scale. In the most optimum bound configuration, the average RMSD ($\langle RMSD \rangle_{bound}$) of siRNA is 19.4 ± 0.4 Å on graphene whereas $\langle RMSD \rangle_{bound}$ of dsDNA is 8.5 ± 0.6 Å. As the binding of siRNA is more on graphene, the siRNA structure deforms leading to a large value of $\langle RMSD \rangle_{bound}$.

D. Unzipping kinetics

In Figures 6(a) and 6(b), we plot the number of contacts for siRNA as well the distance between the two strands of the double stranded siRNA (ds-separation) at three different temperatures. It takes few ns to nucleate the unzipping. Once critical numbers of contacts are created between the siRNA and graphene, unzipping starts from one end (end2 for the current situation). Unzipped bases at one end help to make more contacts with graphene and thereby enhancing the interaction between siRNA and graphene. This facilitates unzipping at the other end. Figure 6(a) shows that it takes almost 3 ns at 300 K and less than 1 ns at 340 K for the critical number of contacts to be created. Once this is done, strong interaction between graphene and siRNA force the rapid unzipping of siRNA as is evident from the rapid increase of ds-separation in Figure 6(b). To get an estimate of the unzipping time (τ), we plot the unzipping probability distributions (f_{hb}) at three different temperatures in Figure 7 and fit them to single exponential functions as done in ref. [70]. This gives rise to $\tau = 9.8$ ns, 8.4 ns and 5.0 ns at temperatures 290 K, 300 K and 340 K, respectively. By fitting the unzipping time as a function of temperature to $\tau = \tau_0 e^{E_a/k_B T}$, we get τ_0 to be 100.8 ps and the activation energy, E_a to be 2.637 kcal/mol or 0.114 eV. Plot of $\ln \tau$ versus $\frac{1}{T}$ and the fit was shown in the inset of Figure 7.

E. Insights from Quantum simulations

To understand the difference in binding affinity of siRNA and dsDNA with graphene we have calculated the binding energy of the graphene/siRNA and graphene/dsDNA miniature complexes using dispersion corrected DFT method (DFT-D). The sequence of the siRNA studied has A:U base pairs at both the ends, which is also the case of most of the confirmed siRNA sequences [71], which are known to open up quite easily as compared to G:C base pairs. It may be noted that most of the DNA/RNA oligonucleotide sequences whose three-dimensional structures in double helical forms are available have G:C base pairs at both the termini [72]. The siRNA sequences need to unzip soon for their functionality and probably that drives design of sequences with terminal loosely bound A:U base pairs. However, it appeared that the dsDNA molecule, containing terminal A:T base pairs does not unzip at physiological condition. In order to check whether this is due to stronger attraction in A:T as compared to A:U base pairs, we have optimized both these base pairs using wB97XD/6-31G** method and found their interaction energies to be -15.80 and -15.91 kcal/mol, respectively. This clearly indicates that the terminal A:U base pair is not weaker one as compared to its DNA counterpart. Thus, the other component of differential interaction, i.e. interactions between Uracil residues and Thymine residues with graphene might be driving the RNA molecules to unzip. We are mainly interested in thymidine-graphene and uridine-graphene complex systems since these are the principal nucleosides, which can differentiate between DNA and RNA. Moreover these nucleosides remain unpaired in the siRNA as well as dsDNA. On analyzing the optimized geometry of the complex systems as shown in Figure 8 (graphene-uridine and graphene-thymidine complex), we find that in both the cases O3'-H3' of the constituent sugar points towards the planar graphene sheet with close approach forming O-H... π contacts. In case of thymidine nucleoside, the closest O3'-H3'...ring center is found to be around 2.54 Å, and the angle \langle O3'-H3'...ring center \rangle is obtained as 129.35°. These distances and angles are sufficient to form O-H... π types of H-bonds. While in case of uridine nucleoside, the O3'-H3'...ring center bond distances are found to be 2.34 Å, and the angle \langle O3'-H3'...C \rangle is obtained as 165.32°, forming significantly stronger H-bond between the graphene and uridine sugar, as compared to that of thymidine sugar complex [73]. The O2 and O4 groups of the thymine and uracil also interact with the graphene sheet, but the magnitudes of interaction seems to be very low as compared to that of O-H... π types of contact. Nevertheless these carbon oxygen atoms can form lone pair... π type of contacts giving extra stabilization [74]. In addition to these contacts, the O2'

may also form H-bond with the graphene, which however was not found in the energy minimized structures, but can not be ignored at physiological temperature and between the oligonucleotides. Furthermore several of 2'-OH groups, which are equivalent to 3'-OH, are present in the siRNA strands and absent in the dsDNA strands. Thus the siRNA strands tend to dissociate from their double helical forms and bind strongly to the graphene sheet.

The BSSE corrected interaction energy has been calculated for all the complex systems and they follows the trends $G > A > U > T > C$. Interaction energy of the graphene-uridine nucleoside is found to be -22.26 kcal/mol, while that of graphene-thymidine nucleoside is found to be -20.30 kcal/mol. So we can infer that uridine nucleoside interacts with the graphene more strongly than that of the thymidine nucleoside. These interaction energy values also well correlate the H-bond lengths and angles values obtained in both the cases. Our previous studies [36] on interactions of the graphene with the nucleobases gives the interaction energy strengths as $G > A > C > T > U$. So it proves that inclusion of sugar in the nucleobases alters the interaction energy strengths, therefore plays significant role in stabilizing the systems due to availability of more hydrogen bond donor sites.

Frequency calculation of the entire complex as well as the isolated systems give no imaginary frequency indicating the structures are at their local minima. Frequency calculation enables us to carry out thermochemical analysis of the system. All the calculations are carried out at 298.15 K and 1 atm. pressure. We have calculated the change in enthalpy and free energy of the systems. The ΔH of graphene-uridine is found to be -26.39 kcal/mol, whereas that of ΔH of graphene-thymidine is calculated to be -23.80 kcal/mol. Similarly the ΔG of graphene-uridine and graphene-thymidine are found to be -11.95 and -10.22 kcal/mol, respectively. As it is well known that the system is more favorable with increase in the negative value of ΔG , graphene-uridine complex is more stable. The formation of stable graphene-uridine nucleoside complex may initiate and enhance the unzipping of the siRNA structure as observed by our counterpart MD simulation studies.

We have also calculated the NBO charges of the thymidine and uridine nucleosides of the graphene-nucleosides systems and compared with the isolated nucleosides. The difference in NBO charges of the major hydrogen bond donor atoms of the nucleosides which interacts with

the graphene sheet are given in Table II. We observed that charge transfer is more significant for the O3'-H3' and O4 atoms for uridine molecule with graphene, since they interact strongly with the graphene sheet. The O2 of thymidine shows negligible amount of charge transfer with the graphene sheet. It may also be noted that due to the methyl group of thymine, close to the O4 atom, the O4 atom of thymine may not be allowed to come close to the graphene plane, thereby reducing its interaction strength. We can conclude that uridine interacts with the graphene sheet more strongly than thymidine, which is well correlated with the hydrogen bond strengths, interaction energy, and thermochemical analysis of the systems.

IV. CONCLUSION

We demonstrated very unusual phenomena of complete siRNA unzipping and binding on graphene substrate. One of the major goals of the current study is to understand the binding mechanism of siRNA/dsDNA on graphene. Our study also shows that siRNA unzips and binds to graphene forming graphene-siRNA hybrid. This allows us to study the siRNA unzipping kinetics. siRNA unzipping is very important in the context of RNAi therapeutics where a short siRNA enters into cell and gets unzipped for its further action. Studying unzipping kinetics through graphene also offers an alternate route to nanopore assisted unzipping where an electric field is applied to translocate dsRNA/dsDNA. The stable graphene-siRNA hybrid may also be used for efficient delivery of siRNA. The complex may penetrate the hydrophobic regions of the bilayer due to hydrophobicity of graphene. Inside the cell, the graphene-siRNA may remain as complex between graphene and two single stranded RNA chains. One of the chains might easily dissociate from the complex whenever a competitive messenger RNA chain approaches the complex. This can silence the required gene. Another interesting observation is that dsDNA of same sequence as siRNA except thymine in place of uracil has less unzipping and less binding on graphene. This interesting property could be used to detect or separate siRNA and dsDNA molecules. We support these findings through long classical MD simulation as well as calculating the relative binding affinity of nucleosides with graphene through dispersion corrected DFT methods. It is shown that the unpaired uracil residues make strongest contacts with the graphene molecule through van der Waals and specific H-bonding interaction involving 2'-OH group of the ribose sugar. These interactions can be responsible for the double helical siRNA to unzip, which are stabilized

subsequently by several such O-H... π interaction. The equivalent double stranded DNA does not have the -OH group and hence remains stable throughout the simulation time. The spontaneous unzipping helps us to study the siRNA unzipping kinetics for the first time. Unzipping time is of the order of 5-10 ns and decreases with increasing temperature. Unzipping time follows Arrhenius behavior and allows us to get an estimate of the energy barriers for the siRNA unzipping. In contrast to the unzipping kinetics study through nanopore unzipping which requires application of voltage and takes longer time [75], unzipping in graphene is very fast and happen spontaneously.

V. ACKNOWLEDGEMENTS

We acknowledge computational resource supported by the DST Centre for Mathematical Biology at IISc. We thank DBT, India for the financial support. SM thank UGC, India for senior research fellowship.

-
- [1] M. Zheng, A. Jagota, E. D. Semke, B. A. Diner, R. S. Mclean, S. R. Lustig, R. E. Richardson, and N. G. Tassi. Nature Materials, 2(5):338–342, (2003).
- [2] M. Zheng, A. Jagota, M. Strano, A. Santos, P. Barone, S. G. Chou, B. A. Diner, M. S. Dresselhaus, R. S. McLean, G. B. Onoa, G. G. Samsonidze, E. D. Semke, M. Usrey, and D. J. Walls. Science, 302(5650):1545–1548, (2003).
- [3] C.-H. Lu, H.-H. Yang, C.-L. Zhu, X. Chen, and G.-N. Chen. Angew. Chem. Int. Ed., 48(26):4785–4787, (2009).
- [4] N. Mohanty and V. Berry. Nano Lett., 8(12):4469–4476, (2008).
- [5] S. Garaj, W. Hubbard, A. Reina, J. Kong, D. Branton, and J. A. Golovchenko. Nature, 467(7312):190–193, (2010).
- [6] G. F. Schneider, S. W. Kowalczyk, V. E. Calado, G. Pandraud, H. W. Zandbergen, L. M. K. Vander-sypen, and C. Dekker. Nano Lett., 10(8):3163–3167, (2010).
- [7] C. A. Merchant, K. Healy, M. Wanunu, V. Ray, N. Peterman, J. Bartel, M. D. Fischbein, K. Venta, Z. Luo, A. T. C. Johnson, and M. Drndic. Nano Lett., 10(8):2915–2921, (2010).
- [8] Z. Liu, M. Winters, M. Holodniy, and H. Dai. Angew. Chem. Int. Ed., 46(12):2023–2027, (2007).
- [9] Z. Liu, K. Chen, C. Davis, S. Sherlock, Q. Cao, X. Chen, and H. Dai. Cancer Res., 68(16):6652–6660,(2008).
- [10] Z. Liu, S. Tabakman, K. Welsher, and H. Dai. Nano Research, 2(2):85–120, (2009).
- [11] C.-H. Lu, C.-L. Zhu, J. Li, J.-J. Liu, X. Chen, and H.-H. Yang. Chem. Commun., 46(18):3116–3118, (2010).
- [12] A. Das, A. K. Sood, P. K. Maiti, M. Das, R. Varadarajan, and C. N. R. Rao. Chem. Phys. Lett., 453(4-6):266–273, (2008).
- [13] N. Varghese, U. Mogera, A. Govindaraj, A. Das, P. K. Maiti, A. K. Sood, and C. N. R. Rao. ChemPhysChem, 10(1):206–210, (2009).
- [14] S. Gowtham, R. H. Scheicher, R. Ahuja, R. Pandey, P. Karna, and P. Shashi. Phys. Rev. B., 76(3):033401, (2007).
- [15] M. Santosh, S. Panigrahi, D. Bhattacharyya, A. K. Sood, and P. K. Maiti. J. Chem. Phys., 136(24):065106, (2012).
- [16] B. Nandy, M. Santosh, and P. K. Maiti. J. Biosci., 37(3):457–474, (2012).

- [17] D. Umadevi and G. N. Sastry. J. Phys. Chem. Lett., 2(13):1572–1576, (2011).
- [18] C. Napoli, C. Lemieux, and R. Jorgensen. Plant Cell, 2(4):279–289, (1990).
- [19] A. Fire, S. Q. Xu, M. K. Montgomery, S. A. Kostas, S. E. Driver, and C. C. Mello. Nature, 391(6669):806–811, (1998).
- [20] J. Couzin. Science, 298(5602):2296–2297,(2002).
- [21] P. D. Zamore, T. Tuschl, P. A. Sharp, and D. P. Bartel. Cell, 101(1):25 – 33, (2000).
- [22] G. Hutvagner and P. D. Zamore. Current Opinion in Genetics & Development, 12(2):225 – 232, (2002).
- [23] Y. Tomari, C. Matranga, B. Haley, N. Martinez, and P. D. Zamore. Science, 306(5700):1377–1380, (2004).
- [24] P. D. Zamore and B. Haley. Science, 309(5740):1519–1524, (2005).
- [25] M. Ghildiyal and P. D. Zamore. Nature Rev. Genet., 10(2):94–108, (2009).
- [26] J. Kurreck. Angew. Chem. Int. Ed., 48(8):1378–1398, (2009).
- [27] A. Tsubouchi, J. Sakakura, R. Yagi, Y. Mazaki, E. Schaefer, H. Yano, and H. Sabe. J. Cell Biol., 159(4):673–683, (2002).
- [28] Y. Z. Huang, M. W. Zang, W. C. Xiong, Z. J. Luo, and L. Mei. J. Biol. Chem., 278(2):1108–1114, (2003).
- [29] V. Vasumathi and P. K. Maiti. Macromolecules, 43(19):8264–8274, (2010).
- [30] X. Zhao. J. Phys. Chem. C, 115(14):6181–6189, (2011).
- [31] W. Lv, M. Guo, M.-H. Liang, F.-M. Jin, L. Cui, L. Zhi, and Q.-H. Yang. J. Mater. Chem., 20(32):6668–6673, (2010).
- [32] K. Novoselov, A. Geim, S. Morozov, D. Jiang, Y. Zhang, S. Dubonos, I. Grigorieva, and A. Firsov. Science, 306(5696):666–669, (2004).
- [33] J. C. Meyer, A. K. Geim, M. I. Katsnelson, K. S. Novoselov, T. J. Booth, and S. Roth. Nature, 446(7131):60–63, (2007).
- [34] S. Panigrahi, A. Bhattacharya, D. Bandyopadhyay, S. J. Grabowski, D. Bhattacharyya, and S. Banerjee. J. Phys. Chem. C, 115(30):14819–14826, (2011).
- [35] R. S. Paton and J. M. Goodman. J. Chem. inf. mod., 49(4):944–955, (2009).
- [36] S. Panigrahi, A. Bhattacharya, S. Banerjee, and D. Bhattacharyya. J. Phys. Chem. C, 116(7):4374–4379, (2012).
- [37] See Supplementary Material Document No. — for figures, plots and discussion on the effect of force

fields for ff99, parmbsc0 and ff10.

- [38] D. A. Case, T. A. Darden, T. E. Cheatham, III., C. L. Simmerling, J. Wang, R. E. Duke, R. Luo, R. C. Walker, W. Zhang, K. M. Merz, B. Roberts, B. Wang, S. Hayik, A. Roitzberg, G. Seabra, I. Kolossvai, K. F. Wong, F. Paesani, J. Vanicek, J. Liu, X. Wu, S. R. Brozell, T. Steinbrecher, H. Gohlke, Q. Cai, X. Ye, J. Wang, M.-J. Hsieh, G. Cui, D. R. Roe, D. H. Mathews, M. G. Seetin, C. Sagui, V. Babin, T. Luchko, S. Gusarov, A. Kovalenko, and P. A. Kollman. *Amber 11*, (2010).
- [39] Y. Duan, C. Wu, S. Chowdhury, M. C. Lee, G. M. Xiong, W. Zhang, R. Yang, P. Cieplak, R. Luo, T. Lee, J. Caldwell, J. M. Wang, and P. Kollman. *J. Comput. Chem.*, 24(16):1999–2012, (2003).
- [40] Jorgensen, W. L. and Chandrasekhar, J and Madura, J. D. and Impey, R. W. and Klein, M. L. *J. Chem. Phys.*, 79(2):926–935, (1983).
- [41] A. Perez, I. Marchan, D. Svozil, J. Sponer, T. E. Cheatham, III, C. A. Laughton, and M. Orozco. *Biophys. J.*, 92(11):3817–3829, (2007).
- [42] P. Banas, D. Hollas, M. Zgarbova, P. Jurecka, M. Orozco, T. E. Cheatham, III, J. Sponer, and M. Otyepka. *J. Chem. Theory Comput.*, 6(12):3836–3849, (2010).
- [43] I. Yildirim, H. A. Stern, S. D. Kennedy, J. D. Tubbs, and D. H. Turner. *Journal of Chemical Theory and Computation*, 6(5):1520–1531, (2010).
- [44] Y.-R. Yuan, Y. Pei, H.-Y. Chen, T. Tuschl, and D. J. Patel. *Structure*, 14(10):1557–1565, (2006).
- [45] P. K. Maiti, T. A. Pascal, N. Vaidehi, and W. A. Goddard. *Nuc. Acids Res.*, 32(20):6047–6056, (2004).
- [46] P. K. Maiti, T. A. Pascal, N. Vaidehi, J. Heo, and W. A. Goddard. *Biophys. J.*, 90(5):1463–1479, (2006).
- [47] T. Darden, D. York, and L. Pedersen. *J. Chem. Phys.*, 98(12):10089–10092,(1993).
- [48] J. P. Ryckaert, G. Ciccotti, and H. J. C. Berendsen. *J. Comput. Phys.*, 23(3):327–341, (1977).
- [49] H. J. C. Berendsen, J. P. M. Postma, W. F. Vangunsteren, A. Dinola, and J. R. Haak. *J. Chem. Phys.*, 81(8):3684–3690, (1984).
- [50] S. T. Lin, M. Blanco, and W. A. Goddard. *J. Chem. Phys.*, 119(22):11792–11805, (2003).
- [51] P. K. Maiti and B. Bagchi *Nano Lett.*, 6:2478–2485, (2006).
- [52] S.-T. Lin, P. K. Maiti, and W. A. Goddard, III. *J. Phys. Chem. B*, 114(24):8191–8198,(2010).
- [53] H. Kumar, B. Mukherjee, S.-T. Lin, C. Dasgupta, A. K. Sood, and P. K. Maiti. *J. Chem. Phys.*, 134(12):124105, (2011).
- [54] B. Nandy and P. K. Maiti. *J. Phys. Chem. B*, 115:217–230, (2011).
- [55] P. Koskinen, S. Malola, and H. Hakkinen. *Phys. Rev. Lett.*, 101(11),115502, (2008).

- [56] Discovery Studio 2.0, Accelrys Software Inc. San Diego, CA, USA, (2007).
- [57] G. Schaftenaar and J. Noordik. J. Comput.-Aided Mol. Des., 14(2):123–134, (2000).
- [58] J.-D. Chai and M. Head-Gordon. Phys. Chem. Chem. Phys., 10(44):6615–6620, (2008).
- [59] M. J. Frisch, G. W. Trucks, H. B. Schlegel, G. E. Scuseria, M. A. Robb, J. R. Cheeseman, G. Scalmani, V. Barone, B. Mennucci, G. A. Petersson, H. Nakatsuji, M. Caricato, X. Li, H. P. Hratchian, A. F. Izmaylov, J. Bloino, G. Zheng, J. L. Sonnenberg, M. Hada, M. Ehara, K. Toyota, R. Fukuda, J. Hasegawa, M. Ishida, T. Nakajima, Y. Honda, O. Kitao, H. Nakai, T. Vreven, J. A. Montgomery, Jr., J. E. Peralta, F. Ogliaro, M. Bearpark, J. J. Heyd, E. Brothers, K. N. Kudin, V. N. Staroverov, R. Kobayashi, J. Normand, K. Raghavachari, A. Rendell, J. C. Burant, S. S. Iyengar, J. Tomasi, M. Cossi, N. Rega, J. M. Millam, M. Klene, J. E. Knox, J. B. Cross, V. Bakken, C. Adamo, J. Jaramillo, R. Gomperts, R. E. Stratmann, O. Yazyev, A. J. Austin, R. Cammi, C. Pomelli, J. W. Ochterski, R. L. Martin, K. Morokuma, V. G. Zakrzewski, G. A. Voth, P. Salvador, J. J. Dannenberg, S. Dapprich, A. D. Daniels, . Farkas, J. B. Foresman, J. V. Ortiz, J. Cioslowski, and D. J. Fox. Gaussian 09 Revision A.1. Gaussian Inc. Wallingford CT (2009).
- [60] S. Boys and F. Bernardi. Molecular Physics, 19(4):553–566, (1970).
- [61] A. E. Reed, L. A. Curtiss, and F. Weinhold. Chem. Rev., 88(6):899–926, (1988).
- [62] A. E. Reed, R. B. Weinstock, and F. Weinhold. J. Chem. Phys., 83(2):735–746, (1985).
- [63] J. E. Carpenter and F. Weinhold. J. Mol. Struct.-Theochem, 46:41–62, (1988).
- [64] D. Voet and J. G. Voet. Biochemistry. John Wiley & Sons. Inc.,, 3 edition, (2005).
- [65] M. Santosh and P. K. Maiti. J. Phys.: Condens. Matter, 21(3):034113, (2009).
- [66] M. Santosh and P. K. Maiti. Biophys. J., 101(6):1393–1402,(2011).
- [67] C.-W. Lam, J. T. James, R. McCluskey, and R. L. Hunter. Toxicological Sciences, 77(1):126–134, (2004).
- [68] G. Jia, H. Wang, L. Yan, X. Wang, R. Pei, T. Yan, Y. Zhao, and X. Guo. Environmental Science & Technology, 39(5):1378–1383, (2005).
- [69] D. Cui, F. Tian, C. S. Ozkan, M. Wang, and H. Gao. Toxicology Lett., 155(1):73 – 85, (2005).
- [70] J. Mathe, H. Visram, V. Viasnoff, Y. Rabin, and A. Meller. Biophys. J., 87(5):3205–3212, (2004).
- [71] A. M. Chalk, R. E. Warfinge, P. Georgii-Hemming, and E. E. L. Sonnhammer. Nuc. Acids Res., 33:D131–D134, (2005).
- [72] S. Samanta, S. Mukherjee, J. Chakrabarti, and D. Bhattacharyya. Nuc. Acids Res., 130:115103, (2009).

- [73] S. Panigrahi, R. Pal, and D. Bhattacharyya. *J. Biomol. Struct. Dyn.*, 29(3):541–556, (2011).
- [74] A. Jain, V. Ramanathan, and R. Sankararamakrishnan. *Protein Sci.*, 18(3):595–605, (2009).
- [75] A. Sauer-Budge, J. Nyamwanda, D. Lubensky, and D. Branton. *Phys. Rev. Lett.*, 90(23):238101,(2003).
- [76] W. Humphrey, A. Dalke, and K. Schulten. VMD: Visual molecular dynamics. *J. Mol. Graph.*, 14(1):33–&, (1996).

Figures

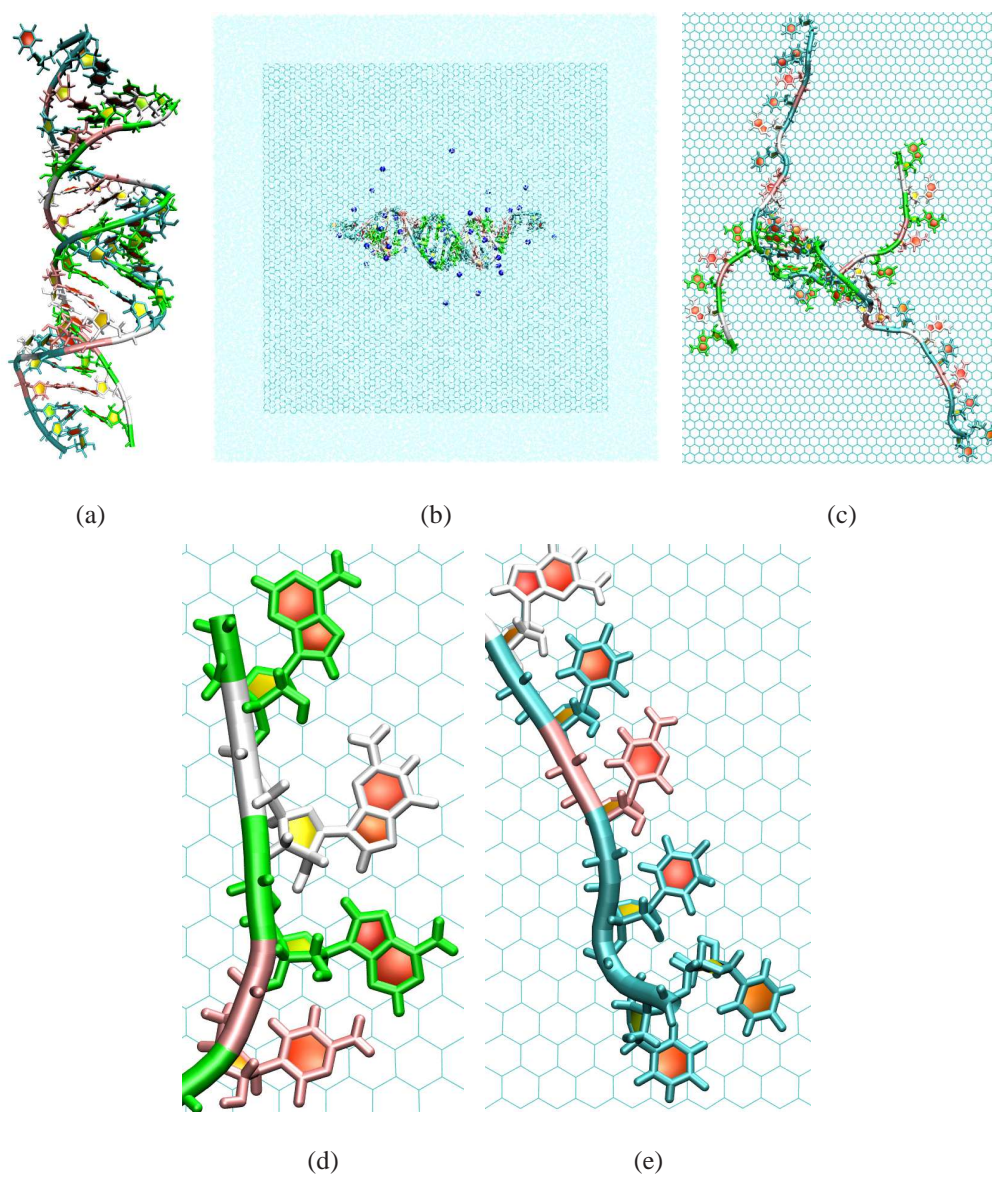


FIG. 1: (a) siRNA crystal structure (pdb code 1F8S) and (b) the initial simulation system setup where siRNA-graphene complex was solvated with water and neutralizing Na^+ counterions. (c) Snapshot of siRNA on graphene after optimum binding. (d) and (e) shows the zoomed part of the completely unzipped siRNA strands whose bases are in $\pi - \pi$ interaction with graphene. The water and counterions were not shown in (c), (d) and (e) for image clarity. The snapshots were rendered using VMD software package [76].

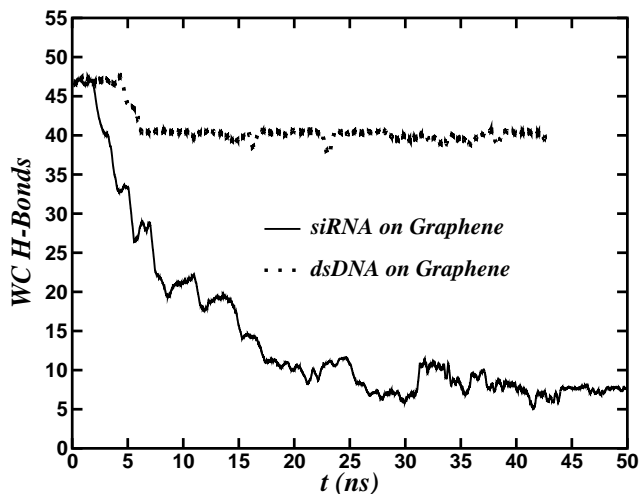


FIG. 2: Number of intact Watson-Crick H-bonds in siRNA and dsDNA as a function of time with graphene. The siRNA has lesser intact WC H-bonds than dsDNA.

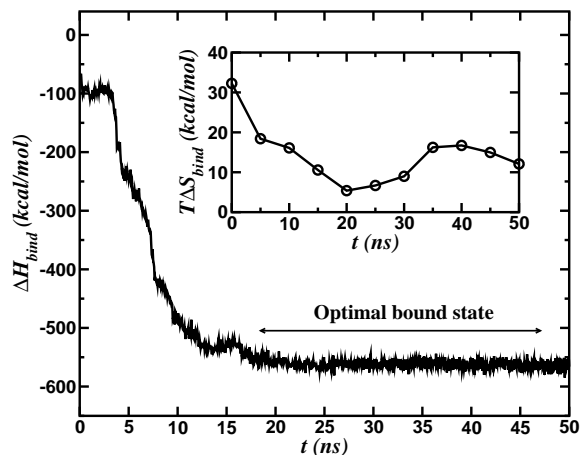


FIG. 3: Enthalpy of siRNA when binding to graphene as a function of time. Correspondingly, the entropy of siRNA is shown in the inset. The enthalpy gets saturated within 18 ns to -562.6 kcal/mol. In the most optimum bound configuration, the binding free energy that includes enthalpy and entropy contributions is -573.0 ± 8.0 kcal/mol.

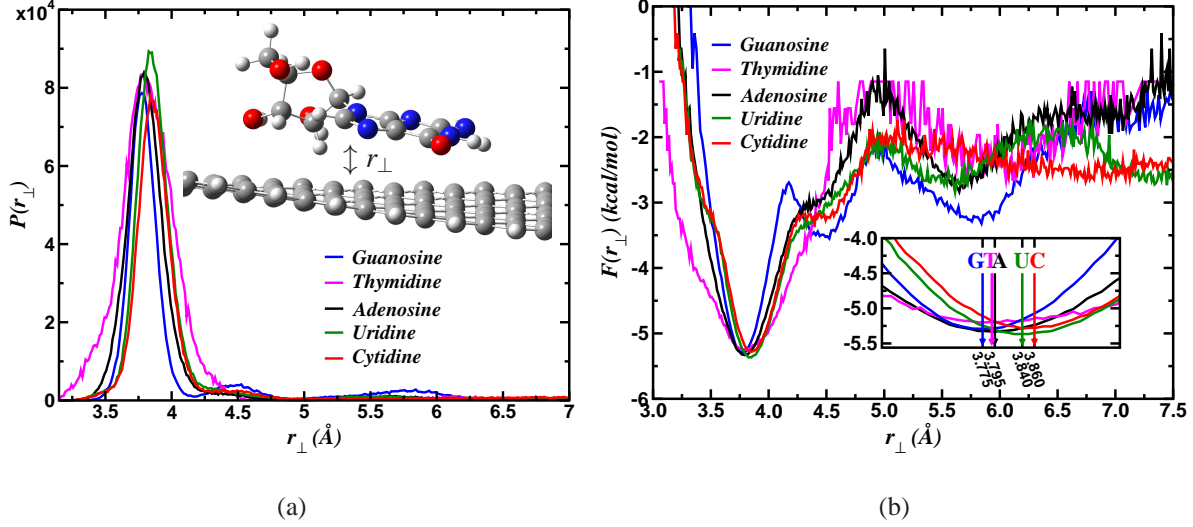


FIG. 4: Nucleosides interaction with graphene from classical MD: (a) Histogram of nucleosides position from graphene surface. In the plot r_{\perp} is the perpendicular distance between the center of masses of nucleoside and graphene as shown. (b) Free energy of the nucleoside-graphene complex as a function of r_{\perp} . Minima in the free energy curve indicates the most optimum bound configuration for the nucleoside-graphene complex. Inset is the zoomed part around free energy minima. The minima occurs at a value in the increasing order for guanosine, thymidine, adenosine, uridine and cytidine. The smaller values of r_{\perp} may imply a larger interaction strength with graphene. Hence guanine has most interaction strength with graphene and in decreasing order thymidine, adenosine, uridine and cytidine.

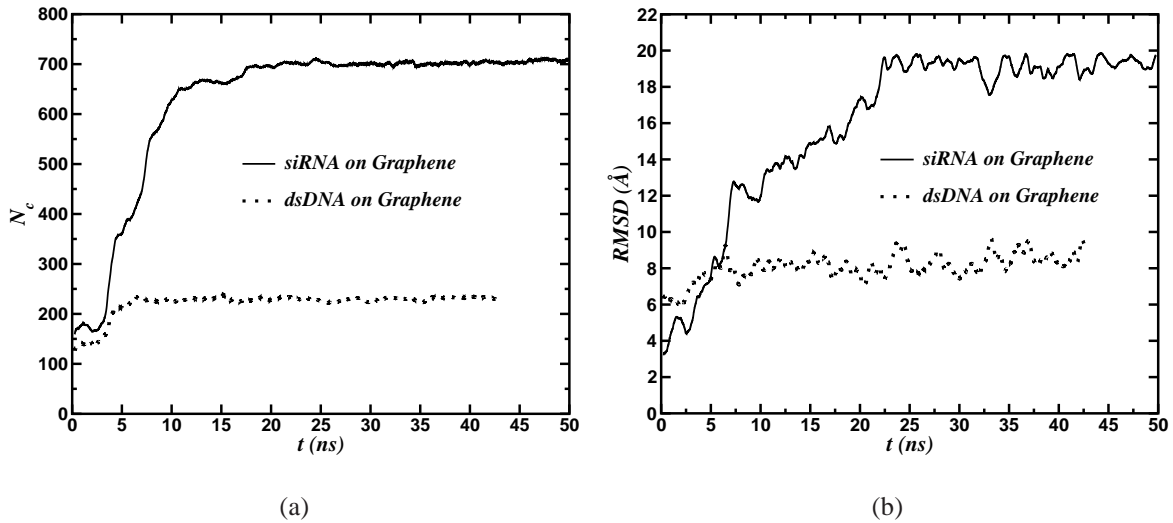


FIG. 5: Number of the close contacts N_c and RMSD of siRNA and dsDNA as a function of time. For siRNA, N_c and RMSD are maximum compared to dsDNA.

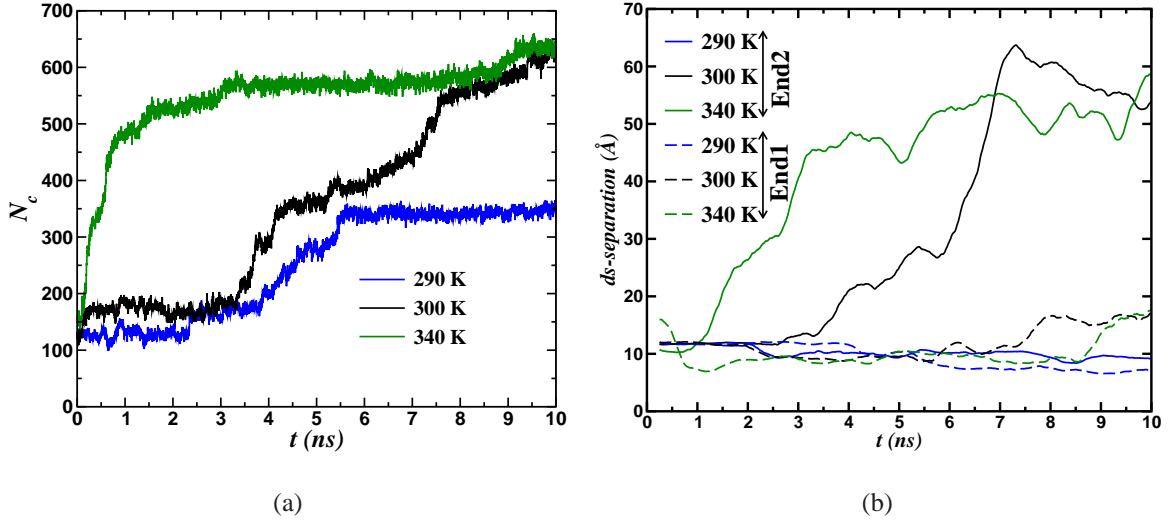


FIG. 6: Temperature effects: (a) Number of close contacts of siRNA on graphene (b) ds-separation of siRNA while unzipping from both the ends.

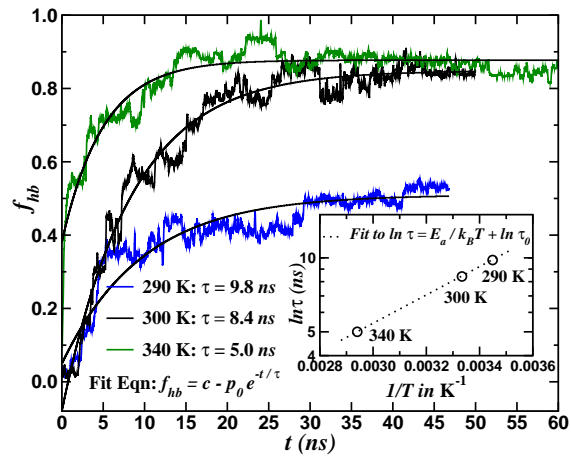


FIG. 7: Unzipping probability denoted by the fraction of broken WC H-bonds, f_{hb} as a function of time for different temperatures.

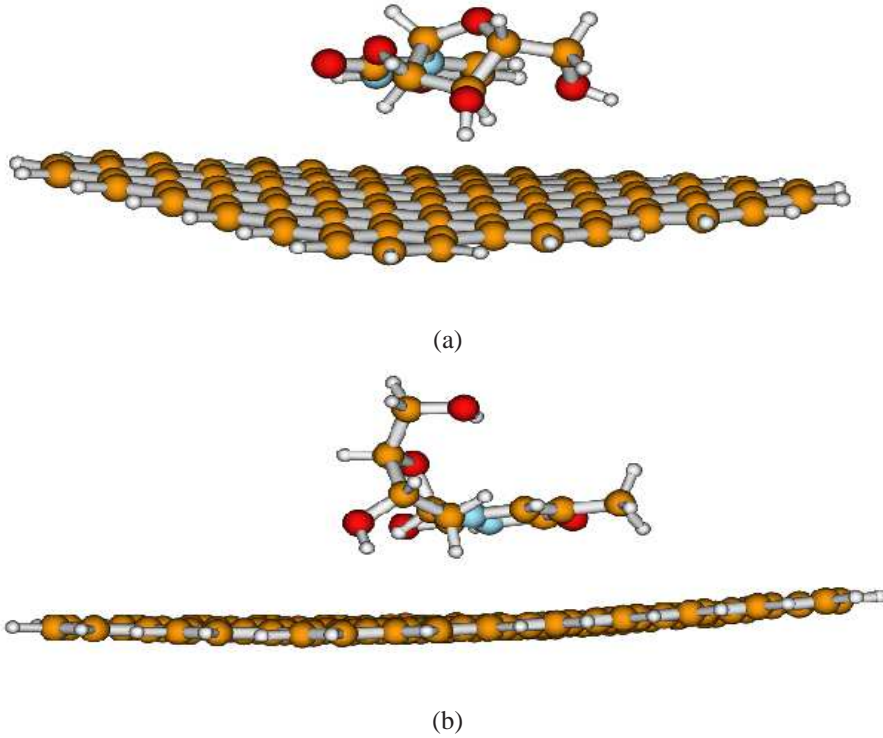


FIG. 8: Quantum DFT-D Optimized geometry of the complex systems: (a) graphene-uridine nucleoside and (b) graphene-thymidine nucleoside.

Tables

TABLE I: Lennard-Jones interaction parameters used for carbon atoms in graphene and counterions Na^+ .

Atom	ϵ/k_B (K)	σ (\AA)
C	43.7	3.40
Na^+	1.41	3.328

TABLE II: Non bonded orbital (NBO) charges of the thymidine and uridine nucleosides

Atom No.	Graphene + Thymidine difference in NBO charge	Graphene + Uridine difference in NBO charge
O3'-H3'	0.005	0.007
O2	0.002	0.000

O4	0.007	0.014
----	-------	-------

Supplementary material for
“Unraveling siRNA Unzipping Kinetics with Graphene”

Santosh Mogurampelly¹, Swati Panigrahi², Dhananjay
Bhattacharyya², A. K. Sood³, and Prabal K. Maiti^{1*}

¹*Centre for Condensed Matter Theory, Department of Physics,
Indian Institute of Science, Bangalore 560012, India*

²*Biophysics Division, Saha Institute of Nuclear Physics, Kolkata 700064, India*

³*Department of Physics, Indian Institute of Science, Bangalore 560 012, India*

arXiv:1207.4569v1 [physics.bio-ph] 19 Jul 2012

*To whom correspondence should be addressed; Electronic address: maiti@physics.iisc.ernet.in

I. FORCE FIELD (FF) EFFECTS

The results of siRNA unzipping mechanism on graphene discussed in the main paper are based on ff99 force field [1]. The ff99 force field has been widely used in the last decade to study the structure and thermodynamics of nucleic acids. However, ff99 is found to produce unphysical torsion angle transitions in ‘ α/γ ’ in longer MD simulations. These irreversible ‘ α/γ ’ transitions introduce severe distortions in nucleic acids. Based on these torsion angle parameterization artefacts, we want to answer if the large structural transitions in siRNA/dsDNA when adsorbed to graphene are due to torsion angle artefacts of ff99. Recently, torsion angle parameters for ‘ α/γ ’ and glycosidic dihedral ‘ χ ’ of nucleic acids have been refined in parmbsc0 [2, 3] and ff10 [4] force fields, respectively. Note that ff10 is equivalent to ff99 + parmbsc0 for DNA and ff99 + parmbsc0 + χ for RNA.

We have studied adsorption of siRNA/dsDNA on graphene with ff99 and parmbsc0. In addition, siRNA adsorption on graphene has been studied with ff10 also and as mentioned for dsDNA, parmbsc0 is equivalent to using ff10. Snapshots and plots of siRNA/dsDNA on graphene with various force fields were shown in Figures 1 and 2, respectively. The major conclusion from these studies is that with parmbsc0 and ff10 also, unzipping and strong adsorption of siRNA on graphene is observed. In comparison, dsDNA has less unzipping and adsorption on graphene compared to the unzipping and adsorption of siRNA. Some of the earlier studies have also demonstrated that ff99 parameters are as good as parmbsc0 set in describing the conformational richness of RNA [5–7]. In our simulation with ff10, less unzipping of siRNA is observed compared to ff99/parmbsc0 (Figure 2(a)). In contrast, with parmbsc0, dsDNA has more unzipping and adsorption than ff99 as it is clear from snapshots (Figure 1) and WC H-bonds, close contacts and RMSD (Figure 2). In spite of these differences, the qualitative features of the siRNA unzipping and adsorption on graphene have been reproduced with all the force fields under consideration. Hence, we conclude that the large structural changes observed with ff99 force field are not because of the artefacts of torsion angle parameters.

-
- [1] Y. Duan, C. Wu, S. Chowdhury, M. C. Lee, G. M. Xiong, W. Zhang, R. Yang, P. Cieplak, R. Luo, T. Lee, J. Caldwell, J. M. Wang, and P. Kollman. J. Comput. Chem., 24(16):1999–2012, (2003).
- [2] A. Perez, I. Marchan, D. Svozil, J. Sponer, T. E. Cheatham, III, C. A. Loughton, and M. Orozco. Biophys. J., 92(11):3817–3829, (2007).
- [3] P. Banas, D. Hollas, M. Zgarbova, P. Jurecka, M. Orozco, T. E. Cheatham, III, J. Sponer, and M. Otyepka. J. Chem. Theory Comput., 6(12):3836–3849, (2010).
- [4] I. Yildirim, H. A. Stern, S. D. Kennedy, J. D. Tubbs, and D. H. Turner. Journal of Chemical Theory and Computation, 6(5):1520–1531, (2010).
- [5] J. Romanowska, J. A. McCammon and J. Trylska. PLoS Comput. Biol., 7, e1002099, (2011).
- [6] I. Besseova, M. Otyepka, K. Reblova and J. Sponer. Phys. Chem. Chem. Phys., 11, 10701-10711, (2009).
- [7] K. Reblova, Z. Strelcova, P. Kulhanek, I. Besseova, D. H. Mathews, K. Van Nostrand, K. I. Yildirim, D. H. Turner and J. Sponer. J. Chem. Theory Comput., 6, 910-929, (2010).

Figures

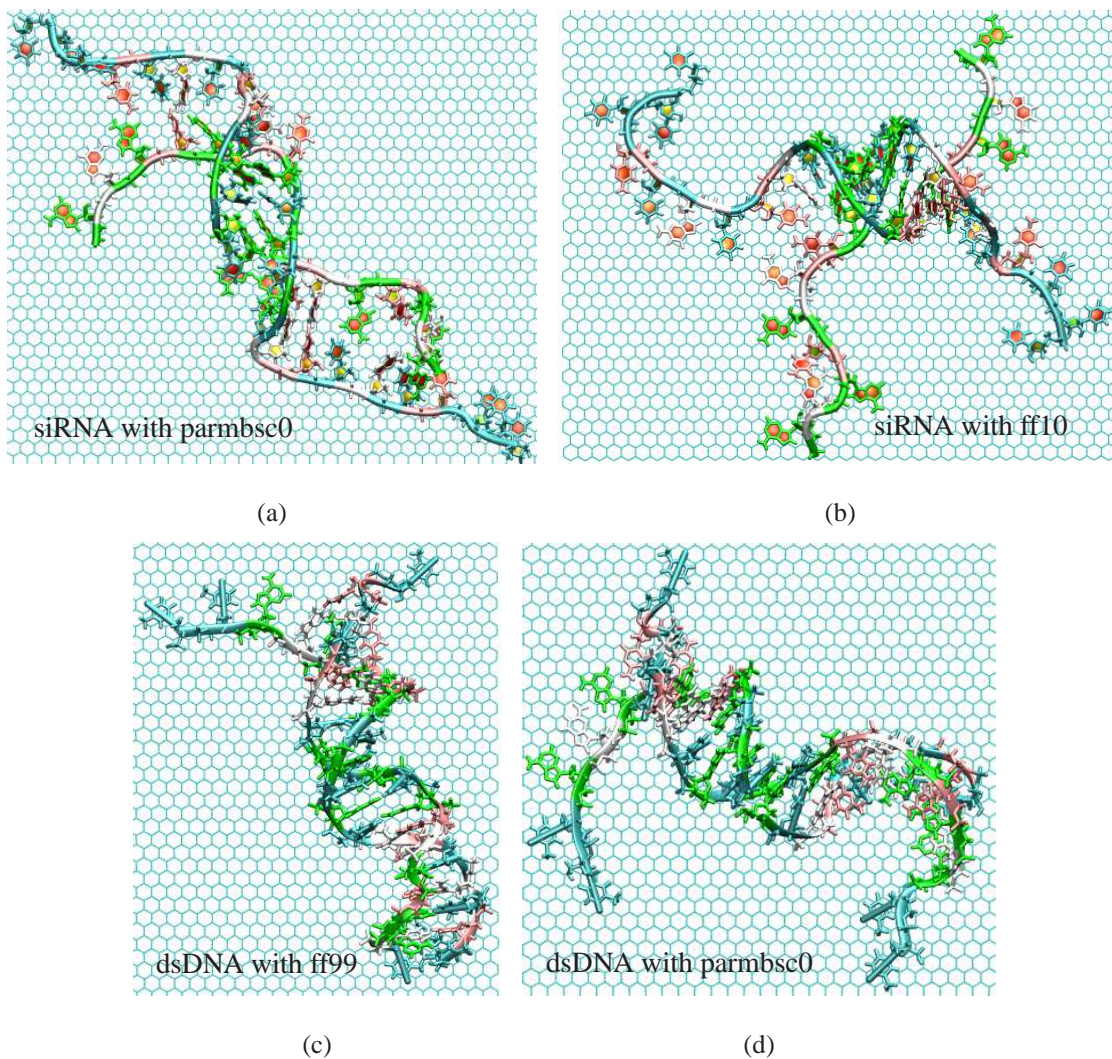
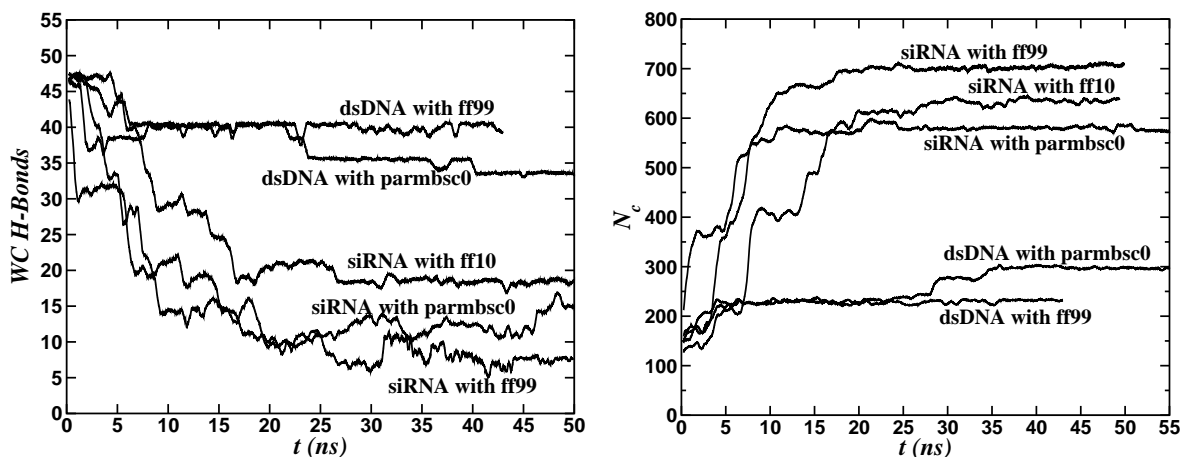
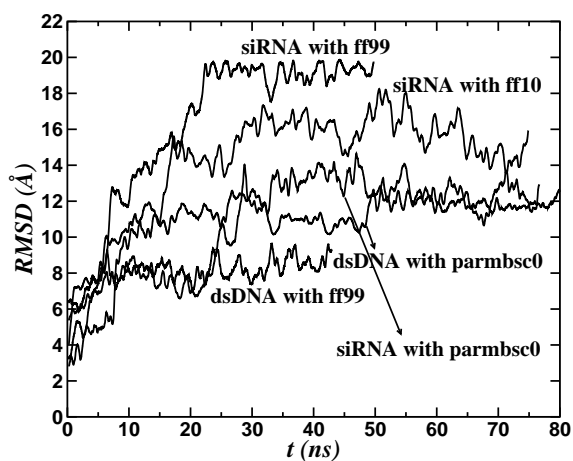


FIG. 1: FF effects: Snapshots of siRNA and dsDNA unzipping and adsorption on graphene using various force fields. The dimension of graphene sheet is $140 \times 140 \text{ \AA}^2$ but only the portion of siRNA/dsDNA adsorption is shown in the figure. These snapshots are taken in the most optimum bound configuration both for siRNA and dsDNA. With ff10 the unzipping of siRNA as can be quantified from the number of intact WC H-bonds (Figure 2(a)) is less but unzipping and adsorption of siRNA on graphene is qualitatively similar to that observed with ff99/parmbsc0. However, parmbsc0 produces more unzipping of dsDNA than ff99 force field (Figure 2(a)).



(a)

(b)



(c)

FIG. 2: FF effects: Time series of the number of intact Watson-Crick H-bonds, close contacts and RMSD of siRNA/dsDNA while adsorbing on graphene for various force fields. These structural quantities verify that the unzipping and adsorption of siRNA/dsDNA on graphene can also be observed using parmbsc0 and ff10. It is interesting to note that RMSD is same for both the siRNA and dsDNA with parmbsc0 while they are very different when using ff99/ff10.